Journal of Nanobiotechnology

RESEARCH

Open Access

MXene-based nanosheet for enhanced glioma therapy via photonic hyperthermia to boost the abscopal effect of radioimmunotherapy

Huan Zhu[1,2†], Zhaoyuan Zhang[1†], Rong Jiang[1†], Liangfu Xu[1], Xiangdi Yang[1], Jie Chen[1], Zhenning Wang[1], Xiao Xu[1*] and Zhigang Liu[1*]

Abstract

Radiotherapy (RT) effectiveness is limited by low DNA damage in tumor cells, surrounding tissue harm, and tumor radioresistance with active DNA repair. Herein, we have engineered a two-dimensional nanomaterial consisting of MXene nanosheets at its core, coated with gold nanorods and a cisplatin shell, and further modified with polyvinyl alcohol, referred to as APMP. The APMP exploits its distinctive electronic properties and photothermal effects to augment radiosensitivity and impede DNA damage repair mechanisms. In vitro experiments demonstrate that APMP elevates reactive oxygen species (ROS) production to approximately 2.6 times higher than that achieved with radiotherapy alone, thereby significantly enhancing the sensitivity to radiotherapy. Combining APMP with photothermal therapy (PTT) and RT is a promising glioblastoma treatment strategy, achieving tumor destruction via localized hyperthermia and overcoming radioresistance. This approach achieves precise tumor targeting, reducing side effects and enhancing therapeutic response in preclinical models. The novel core-shell design enables potent radiotherapy-specific radiosensitizers that drive immunogenic cell death, enhancing glioblastoma combination immunotherapy. This universal strategy heralds a new era in integrating radiotherapy sensitizers with immunotherapy.

†Huan Zhu, Zhaoyuan Zhang and Rong Jiang contributed equally to this work.

*Correspondence:
Xiao Xu
xiaoxu721@smu.edu.cn
Zhigang Liu
zhigangliu1983@hotmail.com

Full list of author information is available at the end of the article

Graphical Abstract

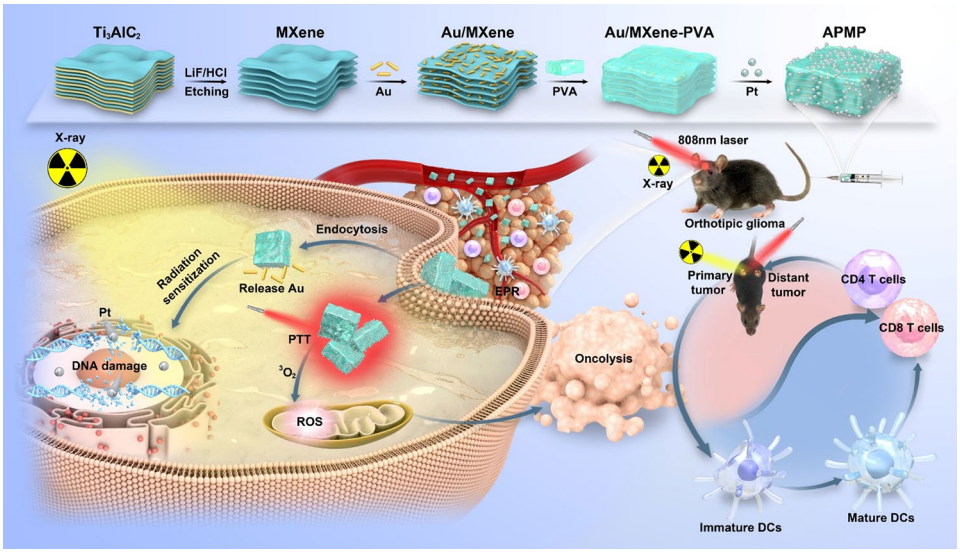

Keywords Mxene, Radiosensitizer, Photothermal therapy, Abscopal effect

Background

Cancer remains a significant challenge in human health, standing as the third leading cause of mortality globally [1]. In 2022, it is that approximately 20 million new cancer cases occurred worldwide, subsequently resulting in a remarkable 9.5 million fatalities attributed to cancer [2]. The conventional modalities for cancer treatment encompass surgery, radiotherapy, and chemotherapy [3–8]. Gliomas, representing the most prevalent form of primary brain neoplasms, constitute approximately 81% of all neurologically-derived tumors [9]. Glioblastoma represents the most common subtype within the glioma spectrum, distinguished by its aggressive malignancy. This subtype carries the poorest prognosis and is responsible for the highest mortality rates among patients diagnosed with gliomas [10].

Radiotherapy, as an integral part of integrated tumor management alongside surgical interventions, has attracted significant research interest. The concurrent administration of radiotherapy and temozolomide chemotherapy represents the standard therapeutic protocol for glioblastoma patients who have undergone surgical intervention within a month. However, the inherently malignant nature and intricate architecture of the brain pose a formidable challenge to complete resection of glioblastoma, predisposing these tumors to frequent recurrence and an unfavorable prognosis [11]. Therefore, improving the cure rate and reducing recurrence are critical concerns that clinicians need to consider for glioblastoma therapy. Radiotherapy, widely acknowledged for its efficacy in cancer treatment, is commonly combined with temozolomide in the clinical management of glioblastoma [12]. However, the effectiveness of this combination in controlling the onset and recurrence of glioblastoma remains suboptimal, as approximately 60% of patients show limited or no response to temozolomide. Namely, temozolomide did not generate desired radiosensitization effect prospectively [13]. Hence, there is an urgent and unmet demand for the development of novel therapeutic agents capable of enhancing the radiosensitizing effects in glioblastoma treatment.

Recently, chemotherapy agents like cisplatin are commonly used as sensitizers to enhance the efficacy of radiotherapy. Furthermore, small molecular compounds, such as sodium glycinate diazole, are being investigated for their radiosensitizing potential [14]. However, although platinum chemotherapeutic agents has been proved to have the potentia for enhancing the therapeutic index of radiotherapy, their use often results in increased side effects due to required dosages. Furthermore, the rapid metabolism of small molecule compounds limits their ability to sustain a therapeutic effect. In contrast, nanoparticles possess advantageous properties such as preferential accumulation in tumor tissues and prolonged retention, facilitated by the enhanced permeability and retention (EPR) effect. This makes nanoparticles an optimal choice for delivering radiosensitizing agents, either as drug carriers or sensitizers themselves. Proverbially, materials containing high atomic number (high-Z) metal elements such as gold, hafnium, tantalum, platinum, and bismuth, among others, are renowned for their robust X-ray absorption capabilities, resulting in an increased

cross-sectional area for radiation absorption and localized higher energy deposition [15]. The interaction of high-Z elements with ionizing radiation can generate reactive oxygen species, leading to direct DNA damage and amplifying the cytotoxic effects of radiotherapy. For instance, HfO_2 nanoparticles, used as a radiosensitizer in Europe, illustrate this effect in the treatment of locally advanced soft tissue sarcoma [16]. Encouragingly, as the only inorganic nanomaterial that has gained clinical approval as a radiosensitizer, hafnium dioxide (HfO_2) is primarily restricted to direct intratumoral injections. However, there exists a notable absence of nanomedical agents engineered for systemic administration via intravenous injection, highlighting an unmet need in the field. The emergence of nanomedical agents amenable to intravenous injection could signify a major stride in the realm of oncological therapeutics, providing a more versatile and potentially more efficacious strategy for the targeted delivery of cancer treatments.

Given the varying radiosensitivity among different tissues and issues such as treatment resistance, radiotherapy has inherent limitations. This has spurred ongoing research into novel technologies and therapeutic approaches. Combining the radiotherapy with other availably antitumor methods appears to be an promising tactic to overcome its limitations. Notably, collaborative therapies have the dual advantage of potentiating the effects of radiotherapy while concurrently mitigating its adverse side effects. The advent of innovative anti-tumor modalities has made the integration of radiotherapy with various approaches possible, including immunotherapy [17], targeted therapy [18], and photodynamic therapy [19], which are either currently utilized or poised for clinical implementation.

Photothermal therapy, an increasingly recognized non-invasive treatment modality, has garnered attention for its simplicity and efficacy in cancer treatment. The synergistic application of radiotherapy and photothermal therapy, however, remains a relatively underexplored area. Cryogenic photothermal therapy, for instance, has been shown to impede DNA repair mechanisms [20], potentially through the downregulation of RAD5 protein expression [21]. Additionally, mild photothermal effects have been reported to ameliorate the hypoxic tumor microenvironment, which can subsequently bolster the efficacy of radiotherapy [22, 23]. Nonetheless, there is still a lack of tactics or exploration that can achieve both radiosensitization and photosensitization simultaneously. High-Z elements enhance radiotherapy sensitivity in tumors through mechanisms such as increasing the photoelectric effect, Compton scattering, improving energy transfer efficiency, and synergistic effects with other treatments [24–26], which was also proved has application feature for photosensitization. In recent years, the two-dimensional material MXene has garnered substantial interest among researchers owing to its favorable biocompatibility and the large specific surface area resulting from its layered structure. These features make it a promising candidate for use as a drug delivery platform or for its intrinsic anti-tumor properties. Extensive research has focused on leveraging MXene's photothermal properties in tumor treatment, producing promising results [27–30]. Interestingly, Capitalizing on the exceptional electronic and ionic conductivity of Mxene, this advanced material has shown promise in enhancing the therapeutic efficacy of radiotherapy. Furthermore, its photothermal characteristics contribute to a synergistic enhancement of the therapeutic outcomes associated with radiotherapy.

Immunotherapy has become a hot research topic in the treatment of glioblastoma (GBM) in recent years [31]. However, glioblastoma (GBM) are "cold tumors" with an immunosuppressive tumor microenvironment (TME), thereby leading to the failure of existing immunotherapeutic regimes [32]. The successful treatment of melanoma using a combination of chemotherapy and immunotherapy indicates that multimodal therapy represents a promising trend in cancer managemen [33]. PTT has substantial promise in the therapeutics of various cancers including GBM [34]. In addition to killing tumor cells directly via photothermal effect, PTT can promote the anti-tumor immune response against GBM via triggering ICD effect and activating immune cells [35]. Meanwhile, ROS play a major role in immune regulation, differentiation, and functions, which can not only kill cancer cells, but also trigger the so-called type II ICD has been developed [36]. The active electronic properties of MXene, when combined with radiotherapy, will generate a substantial amount of ROS. Thus, radiotherapy combin wtih PTT can improve the efficacy of combination therapy with immune checkpoint inhibitors.

In this study, we have synthesized APMP nanomedicines, a novel class of theranostic agents, by integrating gold (Au) and platinum (Pt) onto the surface of Ti_3C_2-Mxene (Unless otherwise specified, 'MXene' hereafter refers to Ti_3C_2), with a subsequent modification using polyvinyl alcohol (PVA). The multifunctional APMP nanoplatform presents several therapeutic advantages: Firstly, the high-Z element titanium (Ti) in Ti_3C_2-Mxene could boost radiosensitivity. Secondly, the inclusion of high-Z elements Au and Pt not only synergistically enhances radiotherapy efficiency but also crucially targets and mitigates DNA repair mechanisms through the nanocarrier's cisplatin payload, thereby addressing radiotherapy resistance [37]. Thirdly, the exceptional optical absorption properties of MXene in the near-infrared spectrum I-II enable effective photothermal therapy. When synergized with radiotherapy, it generates

a significant amount of ROS, which can not only directly kill tumor cells but also induce type II ICD in tumor cells, generate strong immune responses. Furthermore, a mouse model of GBM based on Gl261 cells was constructed to evaluate APMP in mice. APMP could reach the tumor site via the EPR effect. More importantly, APMP + RT + PTT could improve the response rates of PD-1 monoclonal antibody therapy, presenting with the best efficacy among multimodal treatments of combined PTT, radiotherapy, and immunotherapy. Additionally, the in vivo biosafety assessment of APMP underscores its potential for integrated cancer therapy, harnessing both photothermal and radiotherapeutic.

Materials and methods

Chemicals and reagents

The materials used in this study were procured from reputable sources. Titanium aluminum carbide (Ti_3AlC_2) was supplied by Aladdin Industrial Corporation, while gold nanorods were purchased from Nano-Composix, Inc. Cisplatin, in the form of a lyophilized powder, was sourced from MedChemExpress. Polyvinyl alcohol (PVA) was acquired from Sigma-Aldrich. Fetal Bovine Serum (FBS), Dulbecco's Modified Eagle Medium (DMEM), and penicillin-streptomycin solution were all obtained from Gibco, a subsidiary of Thermo Fisher Scientific. Phosphate-buffered saline (PBS) with a concentration of 0.01 M and a pH of 7.4, as well as the Cell Counting Kit-8 (CCK-8), were supplied by Solarbio Science & Technology Co., Ltd. Chemicals of analytical-grade or higher quality chemicals were purchased from reputable local vendors and utilized without further purification. Deionized water, referred to as Watsons water, was consistently employed throughout the all of the studies. Lastly, fluorescein potassium salt was sourced from MCE company.

Synthesis of Ti_3C_2 nanosheets

The Lithium hydrochloric acid/lithium fluoride etching solution was used to selectively remove the aluminum layer from Ti_3AlC_2 so as to synthesize Ti_3C_2 nanosheets. A typical experimental procedure involved the dissolution of 1 gram of lithium fluoride in 20 milliliters of a 9 M hydrochloric acid solution, facilitated by magnetic stirring for 5 min. Thereafter, 1 g of Ti_3AlC_2 was gradually introduced into the etching mixture. The etching reaction was conducted for a total duration of 24 h under a controlled temperature regime set at 35 °C. Post-reaction, the generated Ti_3C_2 nanosheets were dispersed in water adjusted to a pH of 6, and the resulting suspension was subjected to freeze-drying to yield a solid product. The freeze-dried Ti_3C_2 nanosheets were then redispersed in deionized water to establish a stock suspension at a concentration of 10 mg/mL.

Synthesis of Au-Pt@Mxene@PVA nanocomposites

Gold nanorods (AuNRs) were homogeneously mixed with Ti_3C_2 nanosheets at an equal volume ratio and subjected to ultrasonication within an ice bath for 30 min, resulting in the formation of Ti_3C_2@Au nanocomposites. In parallel, PVA was dissolved in a water bath at 60 °C, facilitated by mechanical agitation. Upon complete dissolution of PVA, the Ti_3C_2@Au suspension was added to the PVA solution, and the resulting mixture was stirred using a magnetic stirrer for 4 h to ensure a thorough blend. Thereafter, this cisplatin-containing PBS solution with a final concentration of 1 mg/mL was then incrementally added to the Au@Mxene@PVA mixture under continuous magnetic stirring for a period exceeding 4 h, allowing for the assembly of the nano-drug complex. The reaction mixture was subsequently lyophilized to procure a solid product, which was reserved for use in subsequent experimental applications.

Characterization

The architecture of APMP nanodrugs was examined through transmission electron microscopy (TEM) using a Talos L 120 C microscope operated at 120 kV. A Shimadzu UV-2600 spectrophotometer was uesd to acquire UV-visible absorption spectra. with a Shimadzu UV-2600 spectrophotometer. X-ray diffraction (XRD) data were collected on a Rigaku SmartLab SE X-ray diffractometer, employing a CuKα radiation source. X-ray photoelectron spectroscopy (XPS) studies were carried out employing a Thermo Scientific K-Alpha spectrometer. Particle size and zeta potential assessments were conducted with a NanoBrook Omni particle analyzer. Thermal imaging was documented using a UNI-T UTi320e thermal imager. Near-infrared laser irradiation at 808 nm was provided by a high-power multi-mode pump laser from Changchun Xinye Optoelectronic Technology Co., Ltd., China.

Cellular experiments

The GL261 and GL261-Luc cell lines were procured from the American Type Culture Collection (ATCC). These cell lines were routinely cultured in Dulbecco's Modified Eagle Medium (DMEM), enriched with 10% Fetal Bovine Serum (FBS), and incubated at a temperature of 37 °C within a humidified atmosphere containing 5% CO_2. For the experimental procedures, GL261 cells were plated onto 96-well microplates at an initial seeding density of 2,000 cells/well. Upon achieving confluence and cell adhesion, varying concentrations of the APMP were introduced to the respective wells. After a 24-hour incubation period to allow for drug interaction, the relative cell viability was assessed using the CCK-8 assay, as per the manufacturer's protocol.

In vitro radiotherapy experiments

This study examined the impact of various APMP concentrations on GL261 cell viability. Cells were subjected to APMP treatments at 0, 0.4, 0.6, 0.8, and 1.0 milligrams per milliliter for 24 h, followed by exposure to a 2 Gy (Gy) gamma radiation dose. To assess cell viability, the CCK-8 assay was performed under the manufacturer's instructions. For cell survival analysis, the Live and dead cells were differential stained with AM and PI probes respectively. After a 30-minute incubation with the staining solution, fluorescent microscopy was used to differentiate and quantify viable from non-viable cells.

For in vitro photothermal therapy (PTT) assays, GL261 cells were co-cultured with or without the presence of APMP at a concentration of 0.4 mg/mL for 24 h. After this incubation, the cells were underwent the 808 nm laser irradiation for 10 min, with an untreated control group maintained for comparison. Following the irradiation, the intracellular ROS levels were quantitatively determined using commercial ROS assay kits, and the findings were analyzed through fluorescence microscopy. In cell clone formation assays, GL261 cells were initially treated with various concentrations of APMP. Following a 24-hour incubation, the cells were exposed to 2 Gy gamma radiation. The effectiveness of clone formation was then observed and documented over 7 days. Subsequently, cells were assigned to distinct treatment groups and clone formation rates were assessed following a 7-day extended incubation.

Tumor model

C57BL/6 mice were procured from Spbio Biotechnology Co., Ltd. and maintained in compliance with the approved protocols of the Laboratory Animal Center at Southern Medical University. Briefly, a total of 1×10^5 GL261 cells, suspended in 5 µl of PBS, were stereotactically injected into the frontal lobe of the mice's brains utilizing a brain stereotaxic apparatus. After a 7-day interval, bioluminescence imaging was performed using an IVIS imaging system to capture the resulting emissions.

In vivo PTT/RT combined therapy

Female C57BL/6 mice harboring GL261-Luc tumors were randomly assigned to four experimental cohorts: (1) Control, (2) APMP + PTT, (3) APMP + RT, and (4) APMP + PTT + RT. The administered dosage for groups (2), (3), and (4) was 60 mg/kg. After a 24-hour interval post-injection, mice across the respective groups were subjected to either 808 nm laser irradiation at an intensity of 1.0 W/cm^2 for 10 min and/or a single dose of 8 Gy X-ray irradiation. Tumor progression was monitored and analyzed under established methodologies. Hematoxylin and eosin (H&E) staining of major organs was performed on mice from all treatment groups and the control group at the 28-day mark post-treatment.

Comet assay

The cells were subjected to irradiation (6 Gy), and harvested at 0.5 h. Using the SCGE DNA Damage Detection Kit (KeyGen, China), neutral comet experiments were applied (in which cells were treated with neutral electrophoresis), and propidium iodide (Pl) for staining. The comet photoswere obtained using an inverted fluorescence microscope (Zeiss LSM90) at a magnifcation of x10. CaspLab-Comet Assay software was usedto quantify the tail moments; a score from 10 cells was calculated for eachsample.

Statistical analysis

All the results in this work were presented as mean values ± SD. Statistical analyses were performed with GraphPad Prism 9.5 software. Statistical significances were calculated via Student's t-test or Mann – Whitney U test. $^*p < 0.05$, $^{**}p < 0.01$, and $^{***}p < 0.001$, $^{****}p < 0.0001$.

Result and discussion

APMP characterization

Ti_3C_2 nanodrugs were synthesized through a protocol described in prior literature, adhering to established methods [38]. Nanoparticle analysis revealed a particle size distribution with a mean diameter of 100 nanometers (Fig. 1a). Transmission Electron Microscopy (TEM) was utilized to conduct an exhaustive morphological analysis of the nanodrugs, revealing a distinct nanosheet architecture (Fig. S1), a finding consistent with previous literature observations [39]. Ti_3C_2 displays enhanced stability in aqueous environments, a characteristic that can be ascribed to the presence of surface-adsorbed hydroxyl groups (-OH). Nevertheless, when subjected to saline environments, such as phosphate-buffered saline (PBS), Ti_3C_2 undergoes aggregation and precipitation (Fig. S2). Despite concerted efforts to address aggregation, this phenomenon remains an unresolved issue. The aggregation of Ti_3C_2 and its polymer composites in biological media can be primarily ascribed to the frailty of their intermolecular interactions, significantly compromising stability under such conditions. However, like other inorganic nanometals, their long-term toxicity and biocompatibility for use in biotherapeutics have not yet been clarified. Experimental evidence suggests that modifying the surface of inorganic metal nanoparticles with biocompatible materials can mask their toxicity, thereby achieving biocompatibility [40, 41]. To overcome this challenge, a novel polymerization approach was employed, which involved encapsulating gold (Au) nanorods and cisplatin onto Mxene nanostructures through the use of a PVA matrix. This process resulted in the generation of Au-Pt@

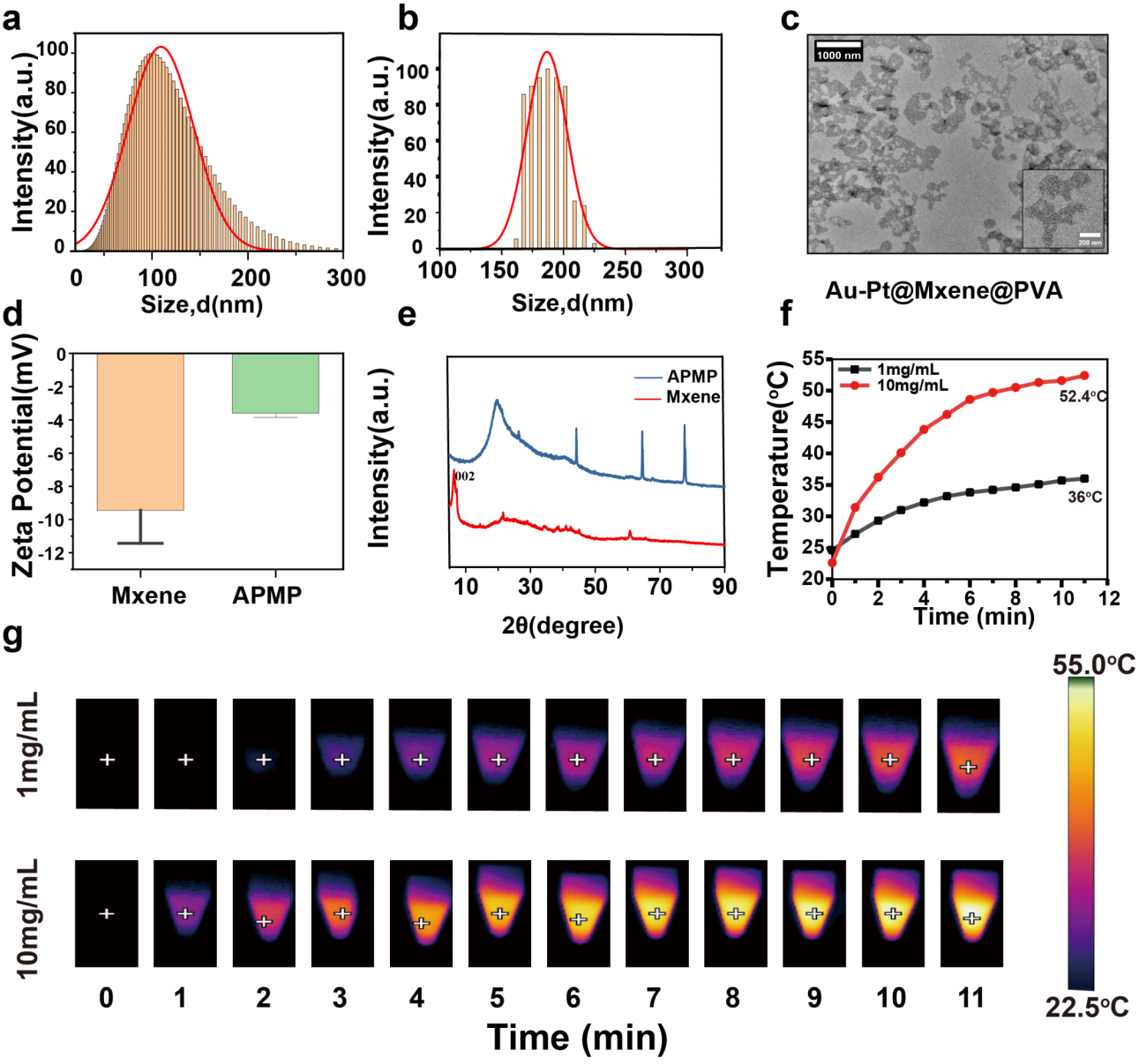

Fig. 1 Characterization of APMP. (**a**) Dynamic light scattering (DLS) size distribution profiles of Ti_3C_2 and (**b**) APMP. (**c**) TEM images of APMP. (**d**) zeta potentials of APMP and Ti_3C_2. (**e**) XRD spectra of Mxene and Au-Pt@Mxene@PVA. (**f**) The photothermal heating curves of APMP at elevated concentrations under irradiation using an 808 nm laser (1 W/cm^2). (**g**) Thermal images of APMP at various concentrations upon laser irradiation

Mxene@PVA (APMP) nanoparticles with an approximate diameter of 180 nm (Fig. 1b). TEM was utilized to examine the morphological features of the synthesized nanoparticles (Fig. 1c). The zeta potential measurements yielded a value of -3.59 ± 0.22 millivolts (Fig. 1d), indicating a potential tendency for particle aggregation. However, the integration of polyvinyl alcohol (PVA) into the Au-Pt@Mxene structure significantly enhanced biocompatibility, a conclusion substantiated by the outcomes of our biocompatibility assays (Fig. S2). X-ray photoelectron spectroscopy (XPS) was employed to investigate the elemental constitution of the APMP nanoparticles. The analysis conclusively confirmed the existence of carbon (C), titanium (Ti), gold (Au) and platinum (Pt) (Figs. S3-7). A high-resolution XPS study of the Ti 2p spectrum disclosed two separate peaks at 465.05 eV and 464.05 eV, characteristic of Ti-O and Ti-C bonding configurations. These observations align with prior literature reports [42]. XRD analysis exhibits the signature peak(002) of Mxene, whereas it is absent for APMP nanoparticles, suggesting that the PVA coating has enveloped the Mxene surface and consequently diminished its biotoxicity (Fig. 1e).

Mxene demonstrates the capacity for efficient photothermal conversion, a prominent attribute that distinguishes this material [43]. In the experimental investigation, the temperature dynamics of an aqueous APMP solution were examined upon exposure to 808 nm laser radiation for a 10-minute duration. A marked temperature rise was observed as the drug concentration increased. Specifically, at a concentration of 10 mg/mL, the solution's temperature escalated by 29.8 °C during this interval. Conversely, at a concentration of 1 mg/mL, the temperature increase was substantially lower, amounting to 11.4 °C (Fig. 1f-g). The Ultraviolet-Visible-Near-Infrared (UV-Vis-NIR) absorption spectrum of the APMP nanoparticles demonstrates a distinctive absorption band within the near-infrared (NIR) region, which spans from 750 to 900 nanometers (Fig. S8).

The absorption intensity of APMP surpasses that of MXene, indicating its superior potential for efficient photothermal conversion (Fig. S8). Increasing the concentration of APMP results in a corresponding enhancement of ultraviolet (UV) absorption intensity (Fig. 2a). Furthermore, the temperature of the APMP solution rises proportionally with laser power (Fig. 2b), demonstrating a linear correlation between laser power input and temperature elevation. This predictable and controllable photothermal conversion efficiency is critical for refining photothermal therapy strategies, particularly in achieving precise temperature regulation for targeted cancer therapies. Additionally, the photothermal stability of APMP was confirmed through eight sequential heating and cooling cycles, which revealed no significant temperature variations (Fig. 2c). The ability to modulate the photothermal properties of APMP enables adaptable treatment planning. In contrast, water exhibited only a minor temperature increase of 2.5 °C (Fig. 2d), further highlighting the exceptional photothermal performance of APMP. While, photothermal therapy not only eradicates cancer cells but also elicits immunogenic responses through Immunogenic Cell Death (ICD) [44].

APMP nanoparticle cellular uptake dynamics and biocompatibility profiling

In this study, we employed bio-electron microscopy to investigate the cellular uptake of APMP nanoparticles in GL261 cells. Our observations revealed the presence of APMP nanoparticles within the lysosomal compartments, indicating that these particles are internalized via lysosome-mediated endocytosis (Fig. 2e).

To evaluate the cytotoxic profile of the synthesized APMP or Au@Mxene@PVA nanoparticles, we executed CCK-8 assays for GL261 cells exposed to different concentrations of nanoparticles. The findings from the CCK-8 assays revealed no substantial cytotoxicity after 24–48 h of exposure, thereby establishing the biosafety of APMP nanoparticles (Fig. 3a-c). The inherent biosafety is indispensable for their suitability in therapeutic interventions.

APMP enhance GBM radiosensitivity in vitro

Expanding upon prior studies that have underscored the radiosensitizing properties of Mxene [45], the integration of high atomic number (Z) elements, specifically gold (Au) and platinum (Pt), within the APMP structure is expected to enhance the therapeutic efficacy of radiotherapy by increasing its therapeutic index. The radiosensitizing capacity of APMP nanoparticles was substantiated by CCK-8 assays (Fig. 3d) and subsequently supported through cell colony formation assays. A dose-dependent relationship is evident, suggesting a direct correlation between the concentration of APMP and the intensified toxic effects observed following radiotherapy in cells (Figs. S9–S10). The optimal working concentration of 0.4 mg/mL was chosen for subsequent cellular investigations due to its ability to strike a balance between enhancing therapeutic effectiveness and mitigating potential adverse effects. Notably, the application of radiotherapy in conjunction with APMP resulted in a substantial decrease in cell colony formation rates when compared to the control group (Fig. 3e-f). The cloning efficiency with X-ray irradiation alone is 56.40%, while the cloning efficiency with APMP plus radiation therapy (RT) is 10.43% and $RER_{2Gy} = 5.40$. ($RER_{xGy}=SF_{xGy,\ control}/SF_{xGy,\ NP)}$ [46]. Based on the sensitization enhancement ratio (SER) calculated via a multitarget single-hit model was 1.08 (Fig. S11), indicating the preferable radiosensitization effect of APMP.

Calcein-AM (green) and Propidium Iodide (PI; red) co-stained images were employed to substantiate the efficacy of radiotherapy on Gl261 cells that had been incubated with APMP nanocomposites following exposure to 2 Gy of X-ray irradiation.

The control and APMP samples demonstrated an absence of appreciable red fluorescence. Conversely, the APMP combined with the RT group exhibited a substantially increased intensity of red fluorescence (Fig. 3g), suggesting the enhanced antitumor efficacy of APMP + RT. The results from the reactive oxygen species (ROS) assay offered further validation, demonstrating a statistically highly significant 2.6-fold augmentation in ROS production in the group treated with the combination of APMP and radiotherapy compared to radiotherapy treatment alone (Fig. 3h-i).

Photothermal therapy (PTT) has emerged as a complementary strategy for tumor management, primarily by exploiting light energy to induce localized heating, thereby mitigating hypoxia within the tumor microenvironment [47]. The live/dead cell staining assays revealed that the number of deceased cells in the APMP + PTT

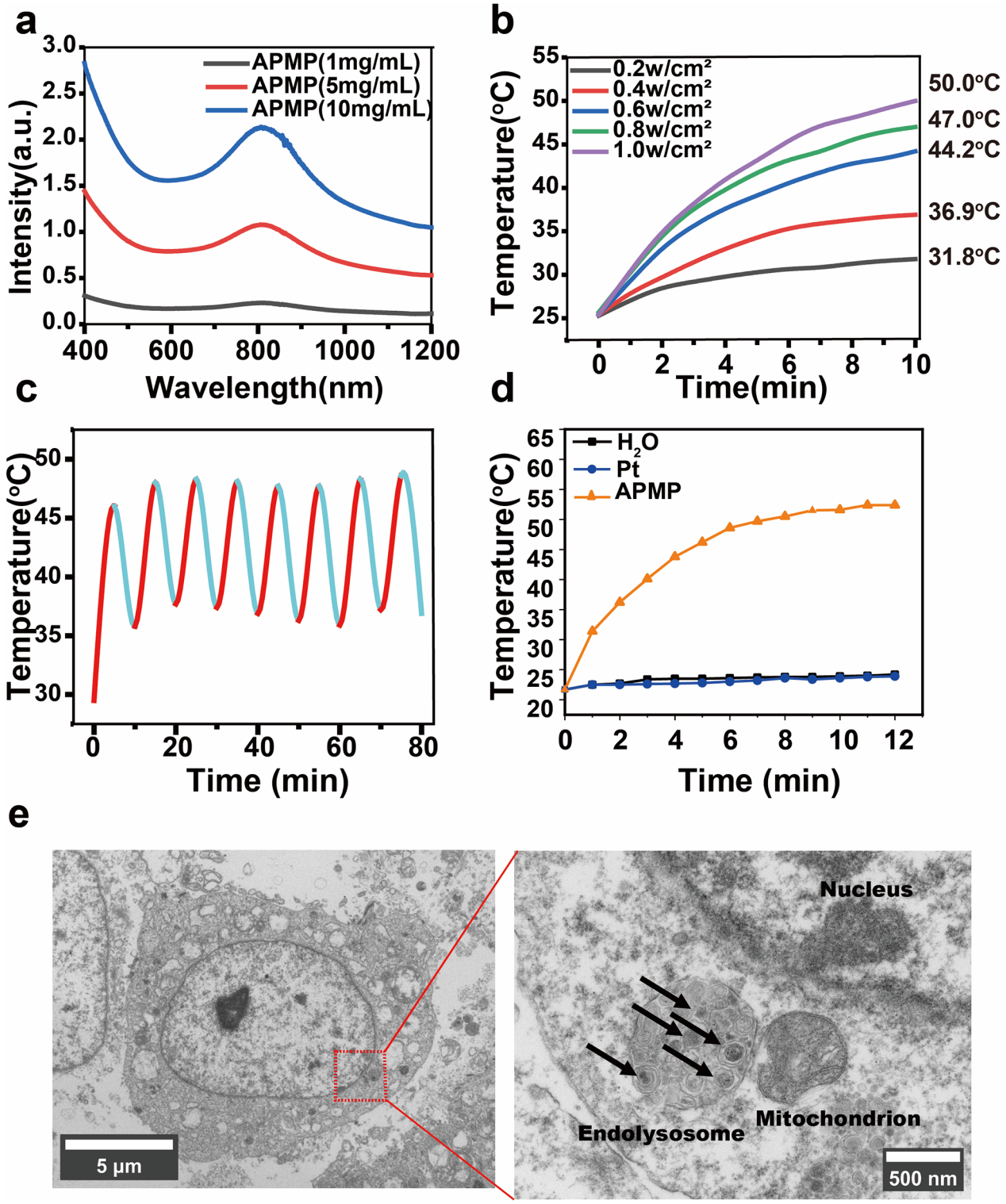

Fig. 2 Optical properties of APMP nanocomposites. (**a**) UV-Visible-NIR absorption spectra of APMP nanosheets in different concentration. (**b**) The photothermal heating curves of the APMP-dispersed aqueous suspension at 10 mg/mL using different power densities. (**c**) Photostability of the APMP nanosheets in water under 808 nm laser irradiation for eight cycles. (**d**) The photothermal heating curves of pure water, APMP, and Cisplatin solution under irradiation using an 808 nm laser (1 W/cm^2). (**e**) A TEM image of GI261 cells incubated with APMP NPs, showing many NPs were observed in lysosomes

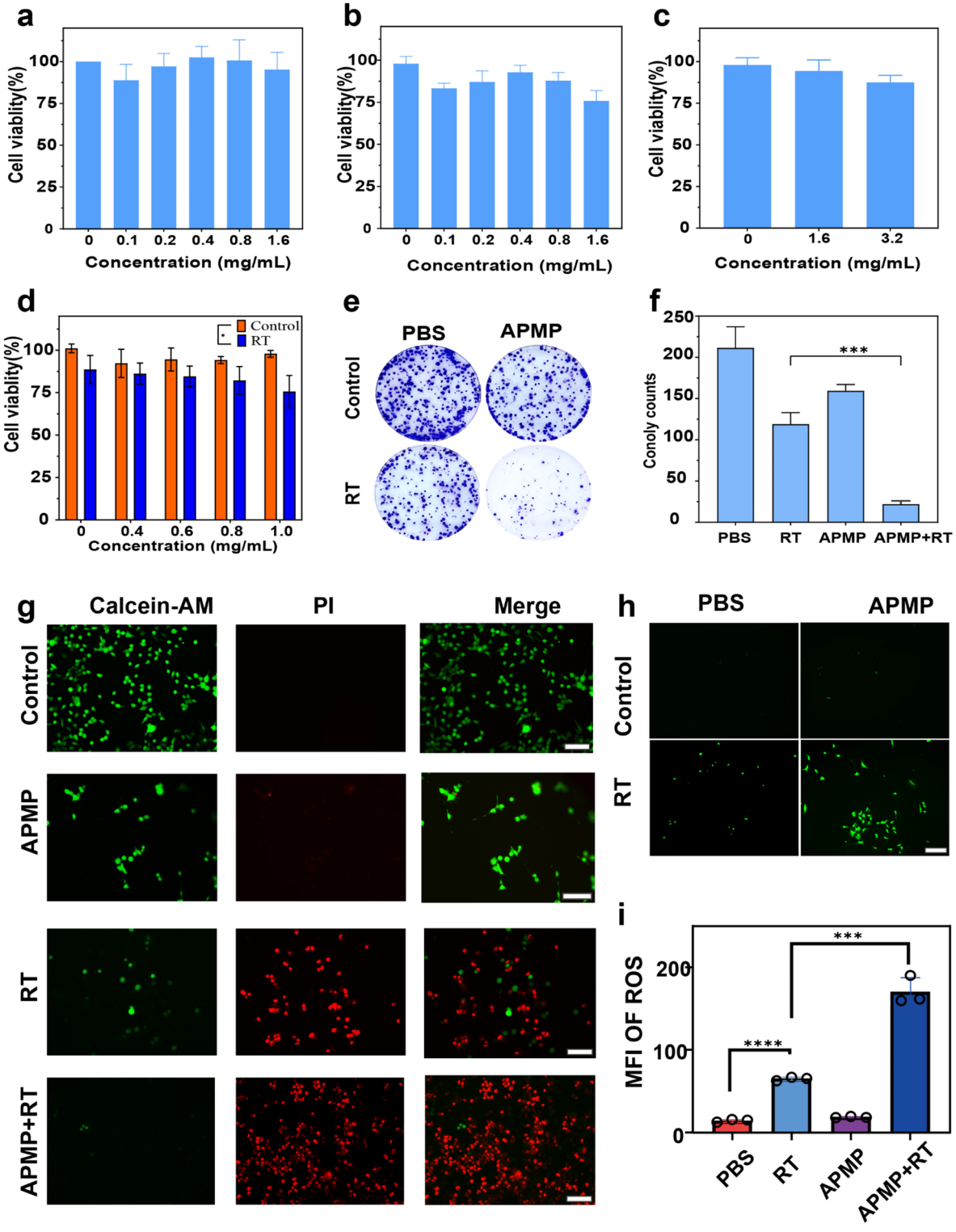

Fig. 3 In vitro cell experiments. (**a**) Relative viabilities of GL261 cells after being incubated with various concentrations of APMP for 24 h and (**b**) 48 h. (**c**) Relative viabilities of GL261 cells after being incubated with various concentrations of Au@Ti_3C_2@PVA for 48 h. (**d**) Relative viabilities of GL261 cells treated by APMP (0.4 mg/mL) with or without RT (2 Gy). (**e**) Representive images of colony formation of Gl261 cells treated with PBS or APMP combined with or without RT (2 Gy). (**f**) Number of GL261 cell colonies in the colony-formation assay. (**g**) Fluorescence images of live (green) and dead (red) cells stained by Calcein-AM and PI after being treated with PBS or Ti_3C_2@Au with the X-irradiation or not. Scale bar, 100 μm. (**h**) Generation of ROS within GL261 cells with different pretreatment by fluorescence microscope observation. Scale bar, 100 μm. **i**) Calculation of mean fluorescence intensity (MFI) of ROS was detected by ImageJ based on DCFH-DA (green) as a probe. Error bars denote standard errors ($n = 3$). *$P < 0.05$,***$P < 0.001$, and ****$P < 0.0001$

group was markedly elevated in comparison to the other groups (Fig. S12). Concurrently, the clonogenic survival rate was markedly lower in the same group (Fig. S13). The heightened cell mortality and diminished clonogenic survival in the APMP + PTT cohort suggest a potentiation of PTT's cytotoxic effects by APMP nanoparticles. This observation underscores APMP's capacity to augment tumor ablation via photothermal therapy. Furthermore, experimental evaluation of Reactive Oxygen Species (ROS) revealed a substantial increase in ROS generation in the APMP + Laser group, compared to the remaining groups, indicating the potential of APMP to function as a photosensitizer (Fig. S14). The production of reactive oxygen species (ROS) by Ti_3C_2 nanosheets can be primarily ascribed to the mechanism of photoexcited electron energy transfer from Ti_3C_2 to ground-state triplet oxygen ($^3O_2$) [48].

The results indicate that after four hours of irradiation, the expression of γ-H2AX in GL261 cells significantly increased in the AMPM + RT group compared to both the AMPM group and the RT group, as well as the control group. This suggests that the combination of AMPM and RT enhances DNA damage(Fig. 4a, b). Additionally, the induced apoptosis and necrosis after each treatment were evaluated (Fig. 4c, d), in which the proportion of apoptotic cells in the APMP + RT group of 15.52% was higher than that in the control group of 6.91%, verifying the existence of cell apoptosis in this mode of treatment. We conducted the DNA-neutral comet assay that detects DSBs at the individual cell level and analyzed comet formation under neutral conditions in Gl261 cells at 0.5 h after irradiation. The results showed that the tail moments in the APMP + RT group were longer than those in the control group (Fig. 4e, f).

Subsequently, we assessed the hemolytic behavior of the drug formulation. Neither the phosphate-buffered saline (PBS) control nor the APMP group displayed any considerable hemolysis, whereas exposure to pure water led to appreciable hemolysis. Concomitantly, escalating the drug concentration does not exhibit a substantial impact on hemolytic activity (Fig. S15). The absence of significant hemolysis in both PBS and APMP samples suggests a low propensity for red blood cell lysis, thereby implying the favorable hemocompatible properties of APMP nanoparticles.

APMP enhances radiotherapy and photothermal ablation of orthotopic glioblastoma in vivo

The combination of radiotherapy with hyperthermia has emerged as a promising strategy to enhance cancer therapy efficacy. Encouraged by the significant cytotoxic outcomes of radiotherapy and hyperthermia in vitro studies, our research aimed to investigate the potential synergistic benefits of integrating photothermal therapy with radiotherapy in an in vivo context. Our meticulously designed in vivo experiments aimed to evaluate the therapeutic outcomes of APMP when combined with radiotherapy and photothermal treatment (Fig. 5a). To evaluate the therapeutic efficacy, tumor-bearing mice were allocated into four distinct groups: a control group, a group receiving APMP (Unless specifically indicated, all administration methods for APMP are via intravenous injection through the tail vein) and radiotherapy (APMP + RT), another group receiving APMP and photothermal therapy (APMP + PTT), and a group undergoing a combination of APMP, radiotherapy, and photothermal therapy (APMP + RT + PTT). The experimental findings demonstrate a marked enhancement in tumor growth suppression when APMP is administered in conjunction with radiotherapy, as compared to the control group receiving solely APMP. This observation implies that APMP potentiates radiotherapy's efficacy. Most notably, the group subjected to the triple therapy combining radiotherapy, photothermal treatment, and APMP (APMP + RT + PTT) exhibited the most substantial tumor regression. This result indicates a synergistic therapeutic response, where the collective action of these treatment modalities exceeds their individual effects, leading to an improved anticancer outcome (Figs. 5b, c and S16).

Upon completion of diverse therapeutic interventions, the mice were euthanized compassionately to enable subsequent histological analysis. Specifically, Hematoxylin and Eosin (H&E) staining, a conventional histopathological method, was employed to visualize cellular architecture and evaluate tissue preservation. Remarkably, the cohort subjected to a concomitant regimen of radiotherapy, hyperthermia, and APMP displayed a considerable degree of tumor cell necrosis. Conversely, the remaining groups manifested minimal or no discernible tissue injury, thereby emphasizing the significant therapeutic advantage of the combined treatment strategy (Fig. 5e). To further investigate cell proliferation and apoptosis in tumor tissues, we employed immunohistochemical staining for Ki-67, a nuclear protein associated with cellular proliferation, and the TUNEL assay for detecting DNA fragmentation in apoptotic cells. The experimental findings lend substantial support to the efficacy of the APMP-driven treatment approach in suppressing tumor growth. A notable decrease in the proliferation index, as evidenced by Ki-67 staining, was observed in tumors excised from mice subjected to the triple combination therapy, thereby demonstrating a robust suppression of cellular division and expansion within the tumor microenvironment. Conversely, the TUNEL assay demonstrated an augmented level of apoptosis, with a conspicuous increase in apoptotic cells within the tumor tissue of the treatment group (Fig. 5e). The combined treatment approach demonstrated a reduction in

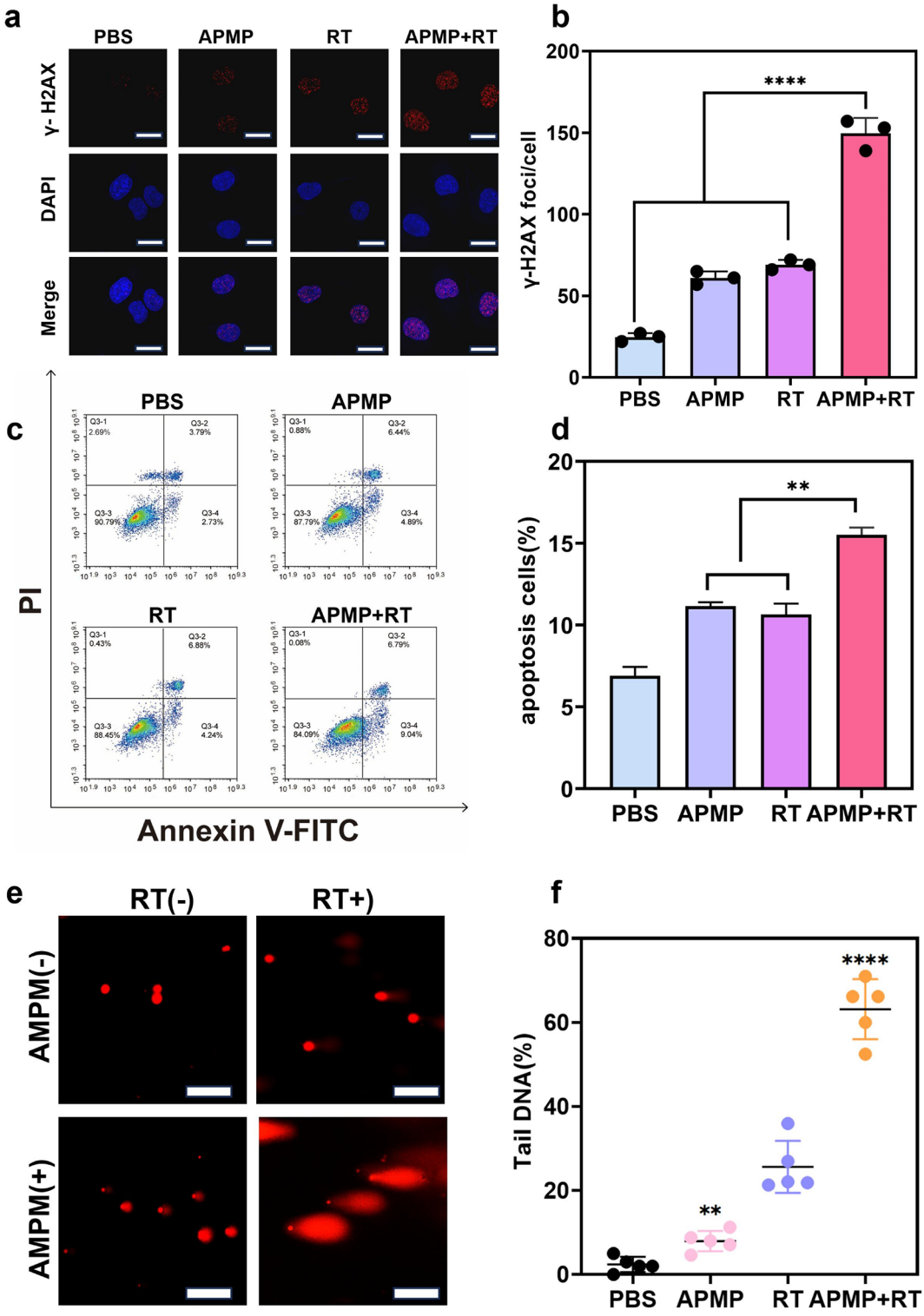

Fig. 4 In vitro cell experiments. (**a**) Representative fluorescence images and (**b**) quantification of γ-H2AX foci immunostaining in Gl261 cells with various treatment. (**c–d**) Flow cytometry analysis of apoptosis of Gl261 cells after different treatments. (**e**) Gl261 cells with various treatment were collected at the indicated time after 6 Gy irradiation for the neutral comet assay. (**f**) CASP-Comet Assay software was used to analyze the tail moment. ($n=5$; scale bar: 50 μm)

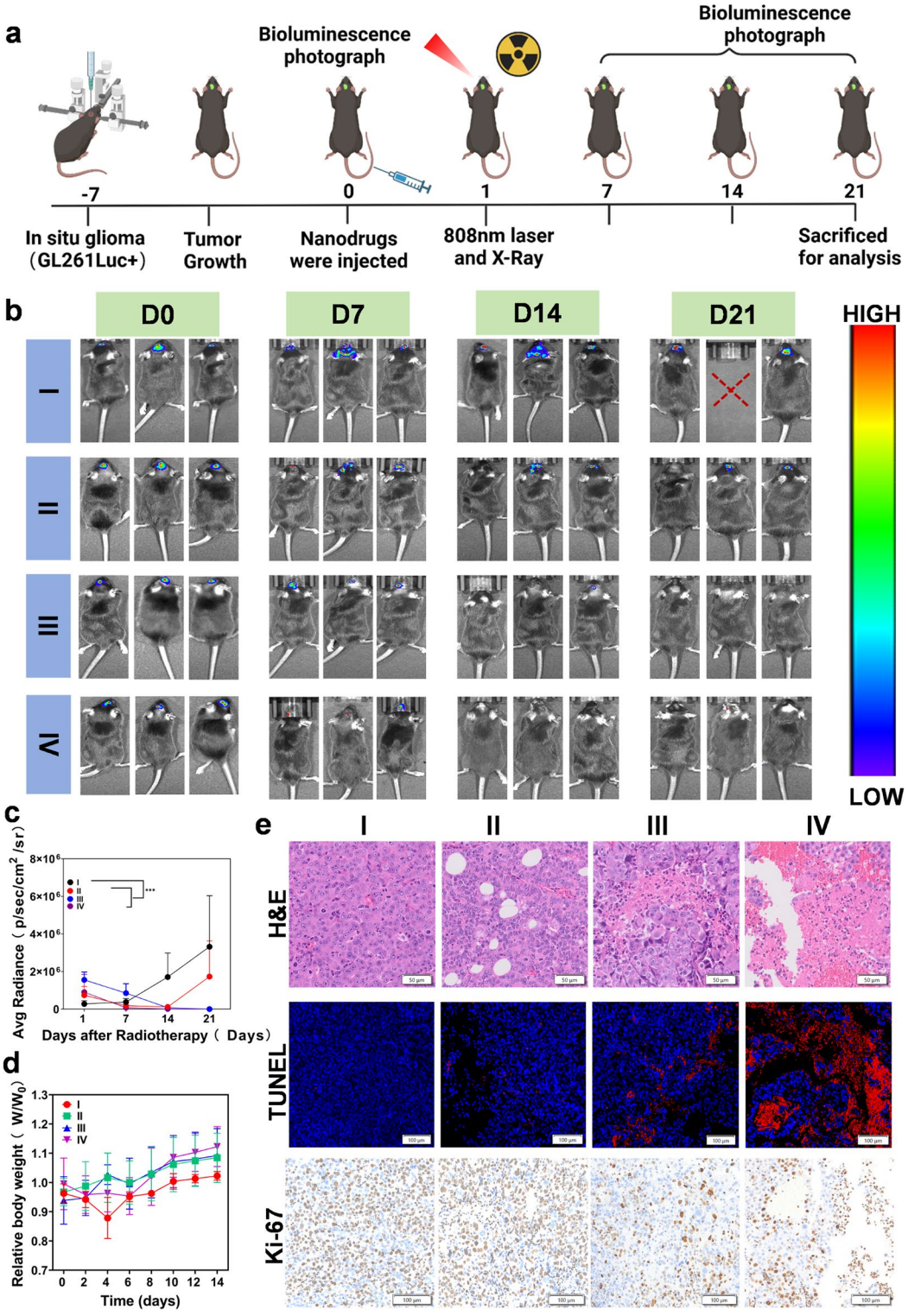

Fig. 5 APMP combination with radiotherapy for treatment of mouse glioblastoma. (**a**) Treatment schedule of Gl261-Luc bearing tumor mice treated with various formulations. (**b**) In vivo representative bioluminescence images showing glioblastoma of intravenously injected GL261-luciferase tumor cells in mice on days 0, 7,14, and 21 according to the treatment schedule. ($n = 3$). (**c**) Quantitative bioluminescence Imaging of Mice. (**d**) Relative Weight Change Curve of Mice Post-Radiotherapy. (**e**) Representative images of tumor sections stained with H&E, TUNEL, and Ki-67. Mice were euthanized following the 14-day treatment period, and tumors were harvested, sectioned, and stained with H&E, TUNEL, and Ki-67. Scale bar, 100 μm. (I-IV represent control, APMP + PTT, APMP + RT, and APMP + RT + PTT respectively)

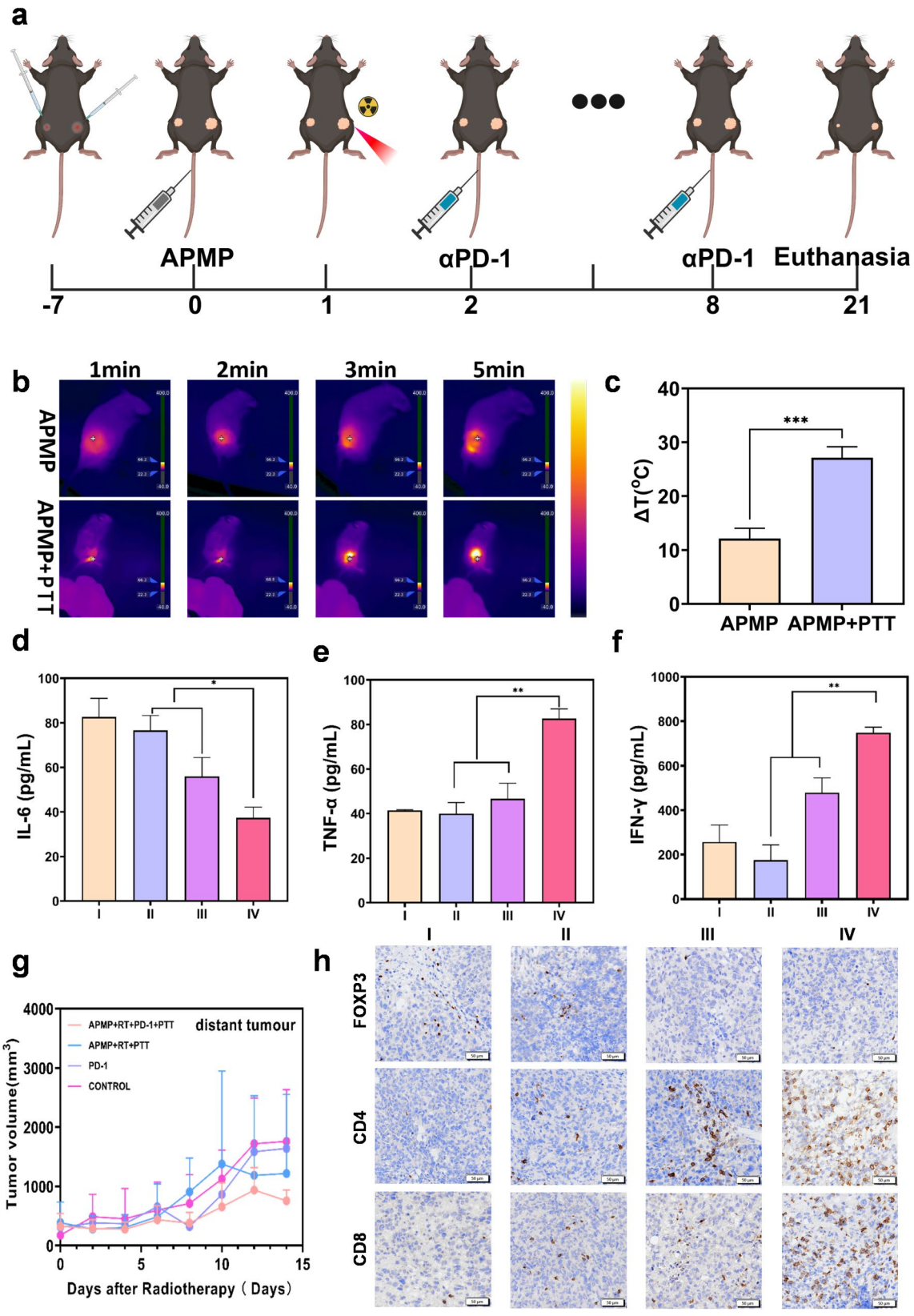

Fig. 6 (See legend on next page.)

(See figure on previous page.)

Fig. 6 Synergistic effects of radiotherapy combined with PTT, APMP and αPD-1 checkpoint blockade. (**a**) A scheme of evaluation of the therapeutic effect on distant tumor. (**b**) Photothermal images and (**c**) Histogram of temperature changes across various treatment groups. (**d**–**f**) The proinflammatory cytokines IL-6, IFN-γ and TNF-α in primary tumor were analyzed by ELISA on the 21th day post-treatment. (**g**) Tumor growth curves of distant tumors. (**h**) IHC of Foxp3, CD4, CD8 of primary tumor collected from mice in different groups on day 21, scale bar: 50 μm. Data were presented as mean ± SD ($n = 3$), *$p < 0.05$; **$p < 0.01$; ***$p < 0.001$. (I-IV represent PBS, α-PD1, APMP + RT + PTT, and APMP + RT + PTT + α-PD1 respectively)

proliferation and an increase in apoptosis, highlighting its efficacy in disrupting tumor growth and viability. These results not only confirm the therapeutic potential of APMP in conjunction with radiotherapy and hyperthermia but also emphasize the importance of a synergistic therapeutic strategy in producing significant anti-tumor effects. The histological evidence of tumor cell necrosis, along with immunohistochemical markers indicating decreased proliferation and increased apoptosis, collectively support the enhanced efficacy of integrating APMP with established cancer treatment modalities.

In nanomedicine, the assessment of in vivo toxicity is paramount. As such, when investigating the prospective applications of APMP in living organisms, its biocompatibility becomes a major focus. To address this, we undertook an extensive evaluation of the in vivo toxicity of APMP-based nanotherapeutics. A critical preliminary indicator of safety is the impact on body weight, which we closely monitored in various mouse cohorts. The observed minimal fluctuations in body weight indicated a seemingly innocuous in vivo safety profile for APMP nanotherapeutics (Fig. 5d). The initial observation signifies an encouraging outcome, suggesting minimal systemic toxicity and the absence of substantial adverse effects on general health associated with APMP administration. To comprehensively evaluate its long-term safety profile, a 21-day treatment regimen was conducted on both healthy rodents and those subjected to radiotherapy-hyperthermia. Upon completion of the treatment period, the animals were humanely euthanized, followed by an exhaustive histopathological examination. Utilizing Hematoxylin and Eosin (H&E) staining, we examined the morphological integrity of multiple vital organs. These assessments yielded no observable tissue damage or pathologic alterations, thereby indicating that APMP does not induce appreciable organ toxicity or architectural disturbances (Fig. S17). Given the intensified scrutiny and rigorous prerequisites for in vivo usage of nanomaterials, this study underscores the indispensable need for comprehensive toxicity evaluations. It is vital to assess the safety of nanomedicines not solely based on acute adverse reactions but also to contemplate possible long-term consequences. Our investigation contributes to this objective by offering insightful data on the safety profile of APMP nanotherapeutics. Ultimately, our findings indicate a conspicuous absence of significant potential toxicity associated with APMP nanomedicine. The absence of significant alterations in body mass, along with the absence of histological evidence for organ damage, suggests that APMP exhibits a favorable in vivo safety profile. Nevertheless, this observation constitutes only one component of a comprehensive assessment. It is crucial to address additional safety concerns in subsequent investigations, including immunogenicity, genotoxicity, and the potential for tissue-specific accumulation. Although this small-scale experimental study demonstrates promising results, further long-term and large-scale investigations are necessary to comprehensively evaluate the overall toxicity and potential side effects, as well as to facilitate the translation of this approach into clinical applications [49].

APMP combined with radiotherapy and hyperthermia enhances GBM immune abscopal effect

Immune checkpoint blockade (ICB)-based immunotherapy is a revolutionary approach that directly eliminates tumor cells through host-adaptive antitumor immunity [50]. However, the response rate of glioblastoma patients to ICB therapy is notably low [51]. Previous research has established that local treatment of tumors exposes a variety of tumor antigens, potentially affecting tumors at distant sites [52, 53]. Combined with the extraordinary potential of nanodrugs in enhancing local responses, we speculate that APMP may also affect the pre-metastatic immune microenvironment to suppress tumor metastasis. Based on these findings, we explored the potential of APMP-based radiotherapy-directed PTT to eradicate metastatic tumors by stimulating the systemic adaptive immune response of organisms in combination with immune checkpoint blockade (Fig. 6a). After injecting APMP and irradiating with an 808 nm laser, the temperature increased by 27.17 °C, which was significantly higher than the 12.13 °C increase observed in the PBS group (Fig. 6b, c). The combination of αPD-1 and APMP + RT + PTT greatly suppressed distant tumor growth compared to treatment with APMP + RT + PTT or αPD-1 alone in Gl261 tumor bearing mice (Fig. 6g). A decrease in IL-6 levels may indicate an enhanced immune response to tumor cells or pathogens following treatment (Fig. 6d). The cytokine secretion, including TNF-α and IFN-γ in serum, was correspondingly increased upon the combination treatment (Fig. 6e, f), indicating a robust antitumor immune response. The combination therapy promoted the infiltration of CD4 + T and CD8 + T cells-cells (Fig. 6h and Fig. S17) in primary tumors and distant tumors. In contrast, the tumoral infiltration of regulatory

T cells (Foxp3 + T cells, namely Tregs), which represent the immunosuppressive tumor microenvironment, dramatically decreased upon combination treatment (Figs. 6h and S18).

Overall, the integration of APMP and PTT targeted by radiotherapy with immunotherapy showed significant promise in the treatment of recurrent glioblastoma. Consequently, future research may focus more on the development of functional nanocarriers that aim to achieve both targeted delivery and enhanced therapeutic effects based on the tumor microenvironment (TME).

The study's findings accentuate the potential of APMP as a multimodal therapeutic compound. The augmented antitumor efficacy witnessed in the combined treatment of APMP, radiotherapy, and near-infrared (NIR) irradiation underscores the importance of employing integrative strategies in cancer management. By capitalizing on the unique attributes of APMP to potentiate both radiotherapy and photothermal therapy, a compelling pathway for designing more efficacious therapeutic regimens has emerged. The preliminary results lay a robust foundation for investigating the underlying mechanisms governing the observed synergistic response. Future investigations must concentrate on elucidating the molecular and cellular processes that underpin APMP's enhancement of radiotherapy and photothermal therapy's effectiveness. Furthermore, an extensive assessment of the long-term safety and biocompatibility of APMP in vivo is crucial for its successful translation into clinical practice. In summary, our in vivo studies have demonstrated the substantial potential of APMP in augmenting the efficacy of radiotherapy and photothermal therapy synergistically. The enhanced antitumor effects in subjects treated with APMP in combination with radiotherapy and photothermal therapy emphasize the promise of multimodal therapeutic strategies in cancer management. Ongoing efforts to optimize APMP and related nanocomposites pave the way for a novel paradigm in cancer therapy, characterized by heightened efficacy, precision, and reduced adverse effects.

Conclusion

In this study, we engineered a multifunctional nanomedicine, Au-Pt@Mxene@PVA (APMP), by leveraging the extensive surface area of Mxene to anchor gold nanorods (Au) and cisplatin. This innovative design significantly enhances the efficacy of radiotherapy and photothermal therapy (PTT), leading to effective tumor cell ablation and substantial improvements in the tumor microenvironment (TME). The synergistic combination of radiotherapy sensitization, cisplatin-mediated chemotherapy, and αPD-1 amplification induces a robust immunogenic cell death (ICD) effect, providing a spatiotemporally coordinated approach with enhanced efficacy and safety compared to conventional therapies.The most significant findings of this study include the demonstration of APMP's ability to generate substantial reactive oxygen species (ROS), modulate the tumor microenvironment (TME), and achieve targeted tumor ablation with minimal off-target effects. These results underscore APMP as a highly promising platform for advanced cancer therapies, particularly in the context of combined treatment strategies. Looking ahead, future research should focus on optimizing the scalability and stability of APMP under physiological conditions, as well as conducting long-term in vivo studies to evaluate its toxicity and therapeutic outcomes. Additionally, efforts should be directed toward engineering functional nanocarriers that further enhance targeted drug delivery and TME modulation. These steps will be critical for translating this innovative nanoplatform into clinical applications and advancing its potential for treating advanced cancers.

Abbreviations

APMP	Au-Pt@Mxene@PVA
CCK-8	Cell counting kit-8
RT	Radiotherapy
ROS	Reactive oxygen species
PTT	Photothermal therapy
PVA	Polyvinyl alcohol
ICD	Immunogenic cell death
EPR	Enhanced permeability and retention
HfO_2	Hafnium dioxide
GBM	Glioblastoma
TME	Tumor microenvironment
FBS	Fetal Bovine Serum
DMEM	Dulbecco's Modified Eagle Medium
PBS	Phosphate-buffered saline
TEM	Transmission electron microscopy
XRD	X-ray diffraction
XPS	X-ray photoelectron spectroscopy
ATCC	American Type Culture Collection
UV-Vis	Ultraviolet-visible

Supplementary Information

The online version contains supplementary material available at https://doi.org/10.1186/s12951-025-03288-z.

Supplementary Material 1

Acknowledgements

Not applicable.

Author contributions

X.X., H.Z., and Z.L. conceived the project. H.Z., Z.Z., R.J., L.X., X.Y., J.C., and Z.W., performed the experiments and analysed the results. All authors discussed the results and edited on the manuscript.

Funding

This study was funded by the Guangdong Basic and Applied Basic Research Foundation Special Projects (Regional Joint Fund-Key Project) (No. 2320191025000040O), the Open Fund of the China Spallation Neutron Source Songshan Lake Science City (No. KFKT2023A02), and the Guangdong Basic and Applied Basic Research Foundation Special Projects (Regional Cultivation Project) (No. 2023A1515140032).

Data availability
No datasets were generated or analysed during the current study.

Declarations

Ethics approval and consent to participate
All animal experiments were performed in accordance with the China Public Health Service Guide for the Care and Use of Laboratory Animals. Experiments involving mice and the protocols were approved by the Laboratory Animal Center at Southern Medical University.

Competing interests
The authors declare no competing interests.

Author details
[1]Cancer Center, Dongguan Key Laboratory of Precision Diagnosis and Treatment for Tumors, The 10th Affiliated Hospital of Southern Medical University, Southern Medical University, Guangzhou 510280, China
[2]Department of Oncology, Affiliated Hospital (Clinical College) of Xiangnan University, Chenzhou, Hunan 423000, China

Received: 4 December 2024 / Accepted: 2 March 2025
Published online: 11 March 2025

References

1. Dagenais GR, Leong DP, Rangarajan S, Lanas F, Lopez-Jaramillo P, Gupta R, Diaz R, Avezum A, Oliveira GBF, Wielgosz A, et al. Variations in common diseases, hospital admissions, and deaths in middle-aged adults in 21 countries from five continents (PURE): a prospective cohort study. Lancet. 2020;395:785–94.
2. Bray F, Laversanne M, Sung H, Ferlay J, Siegel RL, Soerjomataram I, Jemal A. Global cancer statistics 2022: GLOBOCAN estimates of incidence and mortality worldwide for 36 cancers in 185 countries. CA Cancer J Clin. 2024;74:229–63.
3. Tseng CL, Zeng KL, Mellon EA, Soltys SG, Ruschin M, Lau AZ, Lutsik NS, Chan RW, Detsky J, Stewart J, et al. Evolving concepts in margin strategies and adaptive radiotherapy for glioblastoma: A new future is on the horizon. Neuro Oncol. 2024;26:S3–16.
4. Morrison L, Loibl S, Turner NC. The CDK4/6 inhibitor revolution - a game-changing era for breast cancer treatment. Nat Rev Clin Oncol. 2024;21:89–105.
5. Ferrari D, Violante T, Bhatt H, Gomaa IA, D'Angelo AD, Mathis KL, Larson DW. Effect of previous abdominal surgery on robotic-assisted rectal cancer surgery. J Gastrointest Surg. 2024;28:513–8.
6. Bandini A, Calabrò PF, Banchi M, Orlandi P, Bocci G. Metronomic chemotherapy in elderly patients. Curr Oncol Rep. 2024;26:359–76.
7. Tam SY, Wu VWC. A review on the special radiotherapy techniques of colorectal Cancer. Front Oncol. 2019;9:208.
8. Taito M, Taito S, Banno M, Fujiwara T, Okamura H, Tsujimoto H, Kataoka Y, Tsujimoto Y. Voice rehabilitation for laryngeal cancer after radiotherapy: a systematic review and meta-analysis. Eur Arch Otorhinolaryngol. 2019;276:1573–83.
9. Weller M, Wick W, Aldape K, Brada M, Berger M, Pfister SM, Nishikawa R, Rosenthal M, Wen PY, Stupp R, Reifenberger G. Glioma. Nat Rev Dis Primers. 2015;1:15017.
10. Ostrom QT, Gittleman H, Xu J, Kromer C, Wolinsky Y, Kruchko C, Barnholtz-Sloan JS. CBTRUS statistical report: primary brain and other central nervous system tumors diagnosed in the united States in 2009–2013. Neuro Oncol. 2016;18:v1–75.
11. Mei Y, Wang X, Zhang J, Liu D, He J, Huang C, Liao J, Wang Y, Feng Y, Li H, et al. Siglec-9 acts as an immune-checkpoint molecule on macrophages in glioblastoma, restricting T-cell priming and immunotherapy response. Nat Cancer. 2023;4:1273–91.
12. Schaff LR, Mellinghoff IK. Glioblastoma and other primary brain malignancies in adults: A review. JAMA. 2023;329:574–87.
13. Hegi ME, Diserens AC, Gorlia T, Hamou MF, de Tribolet N, Weller M, Kros JM, Hainfellner JA, Mason W, Mariani L, et al. MGMT gene Silencing and benefit from Temozolomide in glioblastoma. N Engl J Med. 2005;352:997–1003.
14. Wu P, Liu J, Sun X, Li X, Xing L, Yu J. Enhanced radiosensitizing by sodium glycididazole in a recurrent esophageal carcinoma tumor model. Oncotarget. 2017;8:63871–80.
15. Sang W, Xie L, Wang G, Li J, Zhang Z, Li B, Guo S, Deng CX, Dai Y. Oxygen-Enriched Metal-Phenolic X-Ray nanoprocessor for Cancer Radio-Radiodynamic therapy in combination with checkpoint Blockade immunotherapy. Adv Sci (Weinh). 2021;8:2003338.
16. Bonvalot S, Rutkowski PL, Thariat J, Carrère S, Ducassou A, Sunyach MP, Agoston P, Hong A, Mervoyer A, Rastrelli M, et al. NBTXR3, a first-in-class radioenhancer hafnium oxide nanoparticle, plus radiotherapy versus radiotherapy alone in patients with locally advanced soft-tissue sarcoma (Act. In.Sarc): a multicentre, phase 2–3, randomised, controlled trial. Lancet Oncol. 2019;20:1148–59.
17. Shiao SL, Gouin KH 3rd, Ing N, Ho A, Basho R, Shah A, Mebane RH, Zitser D, Martinez A, Mevises NY, et al. Single-cell and Spatial profiling identify three response trajectories to pembrolizumab and radiation therapy in triple negative breast cancer. Cancer Cell. 2024;42:70–e8478.
18. Yang YM, Hong P, Xu WW, He QY, Li B. Advances in targeted therapy for esophageal cancer. Signal Transduct Target Ther. 2020;5:229.
19. Zhang M, Cui Z, Song R, Lv B, Tang Z, Meng X, Chen X, Zheng X, Zhang J, Yao Z, Bu W. SnWO(4)-based nanohybrids with full energy transfer for largely enhanced photodynamic therapy and radiotherapy. Biomaterials. 2018;155:135–44.
20. Cheng X, Yong Y, Dai Y, Song X, Yang G, Pan Y, Ge C. Enhanced radiotherapy using bismuth sulfide nanoagents combined with Photo-thermal treatment. Theranostics. 2017;7:4087–98.
21. Huang Q, Zhang S, Zhang H, Han Y, Liu H, Ren F, Sun Q, Li Z, Gao M. Boosting the radiosensitizing and photothermal performance of Cu(2- x)Se Nanocrystals for Synergetic Radiophotothermal Therapy of Orthotopic Breast Cancer. ACS Nano. 2019;13:1342–53.
22. Tang W, Dong Z, Zhang R, Yi X, Yang K, Jin M, Yuan C, Xiao Z, Liu Z, Cheng L. Multifunctional Two-Dimensional Core-Shell MXene@Gold nanocomposites for enhanced Photo-Radio combined therapy in the second biological window. ACS Nano. 2019;13:284–94.
23. Cheng L, Shen S, Shi S, Yi Y, Wang X, Song G, Yang K, Liu G, Barnhart TE, Cai W, Liu Z. FeSe(2)-Decorated Bi(2)Se(3) nanosheets fabricated via cation exchange for Chelator-Free (64)Cu-labeling and multimodal Image-Guided Photothermal-Radiation therapy. Adv Funct Mater. 2016;26:2185–97.
24. Wang S, You Q, Wang J, Song Y, Cheng Y, Wang Y, Yang S, Yang L, Li P, Lu Q, et al. MSOT/CT/MR imaging-guided and hypoxia-maneuvered oxygen self-supply radiotherapy based on one-pot MnO(2)-mSiO(2)@Au nanoparticles. Nanoscale. 2019;11:6270–84.
25. Wang X, Zhang C, Du J, Dong X, Jian S, Yan L, Gu Z, Zhao Y. Enhanced generation of Non-Oxygen dependent free radicals by Schottky-type heterostructures of Au-Bi(2)S(3) nanoparticles via X-ray-Induced catalytic reaction for radiosensitization. ACS Nano. 2019;13:5947–58.
26. Yang S, Han G, Chen Q, Yu L, Wang P, Zhang Q, Dong J, Zhang W, Huang J. Au-Pt nanoparticle formulation as a radiosensitizer for radiotherapy with dual effects. Int J Nanomed. 2021;16:239–48.
27. He PP, Du X, Cheng Y, Gao Q, Liu C, Wang X, Wei Y, Yu Q, Guo W. Thermal-Responsive MXene-DNA hydrogel for Near-Infrared light triggered localized Photothermal-Chemo synergistic Cancer therapy. Small. 2022;18:e2200263.
28. Zhang J, Qin Y, Chen Y, Zhao X, Wang J, Wang Z, Li J, Zhao J, Liu S, Guo Z, et al. Ultrathin 2D As(2)Se(3) nanosheets for Photothermal-Triggered Cancer immunotherapy. ACS Nano. 2024;18:4398–413.
29. Bai L, Yi W, Sun T, Tian Y, Zhang P, Si J, Hou X, Hou J. Surface modification engineering of two-dimensional titanium carbide for efficient synergistic multitherapy of breast cancer. J Mater Chem B. 2020;8:6402–17.
30. Xu Y, Wang Y, An J, Sedgwick AC, Li M, Xie J, Hu W, Kang J, Sen S, Steinbrueck A, et al. 2D-ultrathin MXene/DOXjade platform for iron chelation chemo-photothermal therapy. Bioact Mater. 2022;14:76–85.
31. Sampson JH, Gunn MD, Fecci PE, Ashley DM. Brain immunology and immunotherapy in brain tumours. Nat Rev Cancer. 2020;20:12–25.
32. Wang T, Zhang H, Qiu W, Han Y, Liu H, Li Z. Biomimetic nanoparticles directly remodel immunosuppressive microenvironment for boosting glioblastoma immunotherapy. Bioact Mater. 2022;16:418–32.
33. Huang Y, Shi Y, Wang Q, Qi T, Fu X, Gu Z, Zhang Y, Zhai G, Zhao X, Sun Q, Lin G. Enzyme responsiveness enhances the specificity and effectiveness of nanoparticles for the treatment of B16F10 melanoma. J Control Release. 2019;316:208–22.
34. Chen J, Ning C, Zhou Z, Yu P, Zhu Y, Tan G, Mao C. Nanomaterials as photothermal therapeutic agents. Prog Mater Sci. 2019;99:1–26.

35. Li Z, Lai X, Fu S, Ren L, Cai H, Zhang H, Gu Z, Ma X, Luo K. Immunogenic cell death activates the tumor immune microenvironment to boost the immunotherapy efficiency. Adv Sci (Weinh). 2022;9:e2201734.
36. Zhang M, Shao W, Yang T, Liu H, Guo S, Zhao D, Weng Y, Liang XJ, Huang Y. Conscription of immune cells by Light-Activatable Silencing NK-Derived exosome (LASNEO) for synergetic tumor eradication. Adv Sci (Weinh). 2022;9:e2201135.
37. Routila J, Qiao X, Weltner J, Rantala JK, Carpén T, Hagström J, Mäkitie A, Leivo I, Ruuskanen M, Söderlund J, et al. Cisplatin overcomes radiotherapy resistance in OCT4-expressing head and neck squamous cell carcinoma. Oral Oncol. 2022;127:105772.
38. Alhabeb M, Maleski K, Anasori B, Lelyukh P, Clark L, Sin S, Gogotsi Y. Guidelines for synthesis and processing of Two-Dimensional titanium carbide (Ti_3C_2Tx MXene). Chem Mater. 2017;29:7633–44.
39. Liao T, Chen Z, Kuang Y, Ren Z, Yu W, Rao W, Li L, Liu Y, Xu Z, Jiang B, Li C. Small-size Ti(3)C(2)Tx MXene nanosheets coated with metal-polyphenol nanodots for enhanced cancer photothermal therapy and anti-inflammation. Acta Biomater. 2023;159:312–23.
40. Sharker SM, Kim SM, Lee JE, Choi KH, Shin G, Lee S, Lee KD, Jeong JH, Lee H, Park SY. Functionalized biocompatible WO3 nanoparticles for triggered and targeted in vitro and in vivo photothermal therapy. J Control Release. 2015;217:211–20.
41. Newaj SM, Kashem TB, Ferdous J, Jahan I, Rawshan H, Prionty NJ, Rakib R, Sadman MA, Faruk FB, Reza HM, Sharker SM. Skin Cancer treatment with subcutaneous delivery of Doxorubicin-Loaded gelatin nanoparticles and NIR activation. ACS Appl Bio Mater. 2024;7:6313–24.
42. Chang X, Wu Q, Wu Y, Xi X, Cao J, Chu H, Liu Q, Li Y, Wu W, Fang X, Chen F. Multifunctional Au modified Ti_3C_2-MXene for photothermal/enzyme dynamic/immune synergistic therapy. Nano Lett. 2022;22:8321–30.
43. Hao S, Han H, Yang Z, Chen M, Jiang Y, Lu G, Dong L, Wen H, Li H, Liu J, et al. Recent advancements on photothermal conversion and antibacterial applications over MXenes-Based materials. Nanomicro Lett. 2022;14:178.
44. Lee MS, Park SM, Kim YJ. Photothermal treatment-based heat stress regulates function of myeloid-derived suppressor cells. Sci Rep. 2024;14:18847.
45. Zimmermann M, Gerken LRH, Wee S, Kissling VM, Neuer AL, Tsolaki E, Gogos A, Lukatskaya MR, Herrmann IK. X-ray radio-enhancement by Ti(3)C(2)T(x) MXenes in soft tissue sarcoma. Biomater Sci. 2023;11:7826–37.
46. Subiel A, Ashmore R, Schettino G. Standards and methodologies for characterizing Radiobiological impact of High-Z nanoparticles. Theranostics. 2016;6:1651–71.
47. Li G, Zhong X, Wang X, Gong F, Lei H, Zhou Y, Li C, Xiao Z, Ren G, Zhang L, et al. Titanium carbide nanosheets with defect structure for photothermal-enhanced sonodynamic therapy. Bioact Mater. 2022;8:409–19.
48. Liu G, Zou J, Tang Q, Yang X, Zhang Y, Zhang Q, Huang W, Chen P, Shao J, Dong X. Surface modified Ti(3)C(2) MXene nanosheets for tumor targeting photothermal/photodynamic/chemo synergistic therapy. ACS Appl Mater Interfaces. 2017;9:40077–86.
49. Zhang Y, Xu Y, Li Z, Chen T, Lantz SM, Howard PC, Paule MG, Slikker W Jr., Watanabe F, Mustafa T, et al. Mechanistic toxicity evaluation of uncoated and pegylated single-walled carbon nanotubes in neuronal PC12 cells. ACS Nano. 2011;5:7020–33.
50. Kubli SP, Berger T, Araujo DV, Siu LL, Mak TW. Nat Rev Drug Discov. 2021;20:899–919.
51. Aldape K, Brindle KM, Chesler L, Chopra R, Gajjar A, Gilbert MR, Gottardo N, Gutmann DH, Hargrave D, Holland EC, et al. Challenges to curing primary brain tumours. Nat Rev Clin Oncol. 2019;16:509–20.
52. Yin X, Chen S, Eisenbarth SC. Dendritic cell regulation of T helper cells. Annu Rev Immunol. 2021;39:759–90.
53. Jiang X, Muthusamy V, Fedorova O, Kong Y, Kim DJ, Bosenberg M, Pyle AM, Iwasaki A. Intratumoral delivery of RIG-I agonist SLR14 induces robust antitumor responses. J Exp Med. 2019;216:2854–68.

Publisher's note